

V.B. NEIMASH,<sup>1</sup> V.M. POROSHIN,<sup>1</sup> A.M. KABALDIN,<sup>1</sup> V.O. YUKHYMCHUK,<sup>2</sup>  
P.E. SHEPELYAVYI,<sup>2</sup> V.A. MAKARA,<sup>3</sup> S.YU. LARKIN<sup>4</sup>

<sup>1</sup>Institute of Physics, Nat. Acad. of Sci. of Ukraine

(46, Nauky Ave., Kyiv 03680, Ukraine; e-mail: neimash@gmail.com)

<sup>2</sup>V.E. Lashkaryov Institute of Semiconductor Physics, Nat. Acad. of Sci. of Ukraine

(45, Nauky Ave., Kyiv 03028, Ukraine)

<sup>3</sup>Taras Shevchenko National University of Kyiv, Faculty of Physics

(2, Academician Glushkov Ave., Kyiv 03127, Ukraine)

<sup>4</sup>Public Joint Stock Company “Research and Production Concern Nauka”

(2b, Les’ Kurbas Ave., Kyiv 03148, Ukraine)

PACS 68.47.Fg

## MICROSTRUCTURE OF THIN Si–Sn COMPOSITE FILMS

*Microstructure investigations of thin Si–Sn alloy films were carried out, by using Auger and Raman spectroscopies, X-ray fluorescence analysis, and electron microscopy. The films were produced by the thermal-vacuum coevaporation of Si and Sn. The properties of films with the Sn content ranging from 1 to 5 wt.% are studied. A significant influence of the tin impurity on the formation of a film surface microrelief and nanocrystals in the amorphous matrix is found. The size of quasispherical formations on the film surface can be of the order of 100 nm. The volume fraction of the silicon nanocrystalline phase in a film can reach 90%. The roles of fabrication conditions and growth rate on the distributions of Sn and technological impurities C and O over the film surface and across the film thickness are analyzed.*

*Keywords:* Microstructure of thin composite films, Auger method, Raman spectroscopy.

### 1. Introduction

The progress in the fabrication technologies of photoelectric solar energy converters made the search for effective means of controllable influence on the energy gap width,  $E_g$ , in silicon materials and the study of the process of their transformation from the amorphous state into the nanocrystalline one to be the challenging tasks [1–5]. Doping the silicon structures with isovalent elements of group IV is one of the efficient methods that allow the width  $E_g$  in them to change. It is known that  $E_g$  in the amorphous alloy silicon-tin,  $\text{Si}_{1-x}\text{Sn}_x$ , considerably decreases, as  $x$  grows from 0.001 to 0.5 [6–8], other characteristics of this material being also changed. In particular, the authors of works [8, 9] showed that the electroconductivity of this alloy has an activation energy close to  $E_g/2$  only at small Sn concentrations. As the content of Sn grows in the interval  $0.01 < x < 0.02$ , the transition of the electroconductivity mechanism to the hopping one is observed. The  $\text{Si}_{1-x}\text{Sn}_x$  alloy is known to absorb light by the direct interband transition mechanism [10]. At the same time, it was shown

in work [11] that the addition of another isovalent impurity – carbon – to this alloy changes the absorption mechanism and makes it the indirect-band-gap one.

It is remarkable that, numerically, those and other properties of  $\text{Si}_{1-x}\text{Sn}_x$  alloys differ substantially in works by different authors. As a possible reason of this discrepancy, we may point to different methods of alloy preparation and even different technological regimes in the framework of that or another method. The influence of technological conditions at the alloy formation on its physical properties evidently takes place by means of modifying the alloy microstructure. In particular, the alloy can be completely or partially amorphous, with Sn atoms being located in substitutional positions of a tetragonal [12] or non-tetragonal [8] configuration, with emerging a regular grid or not; the alloy can contain precipitates of Sn atoms [9, 13] or Si crystals [14]. The crystal dimensions and the volume ratio between the amorphous and crystalline phases can also be different.

A considerable role in the formation of a microstructure and properties of silicon-based alloys is played by the relations between the contents of isovalent impurities, the atoms of which have the covalent radius larger or smaller than that of silicon atoms [11, 15, 16]. All the above-mentioned features

© V.B. NEIMASH, V.M. POROSHIN, A.M. KABALDIN,  
V.O. YUKHYMCHUK, P.E. SHEPELYAVYI,  
V.A. MAKARA, S.YU. LARKIN, 2013

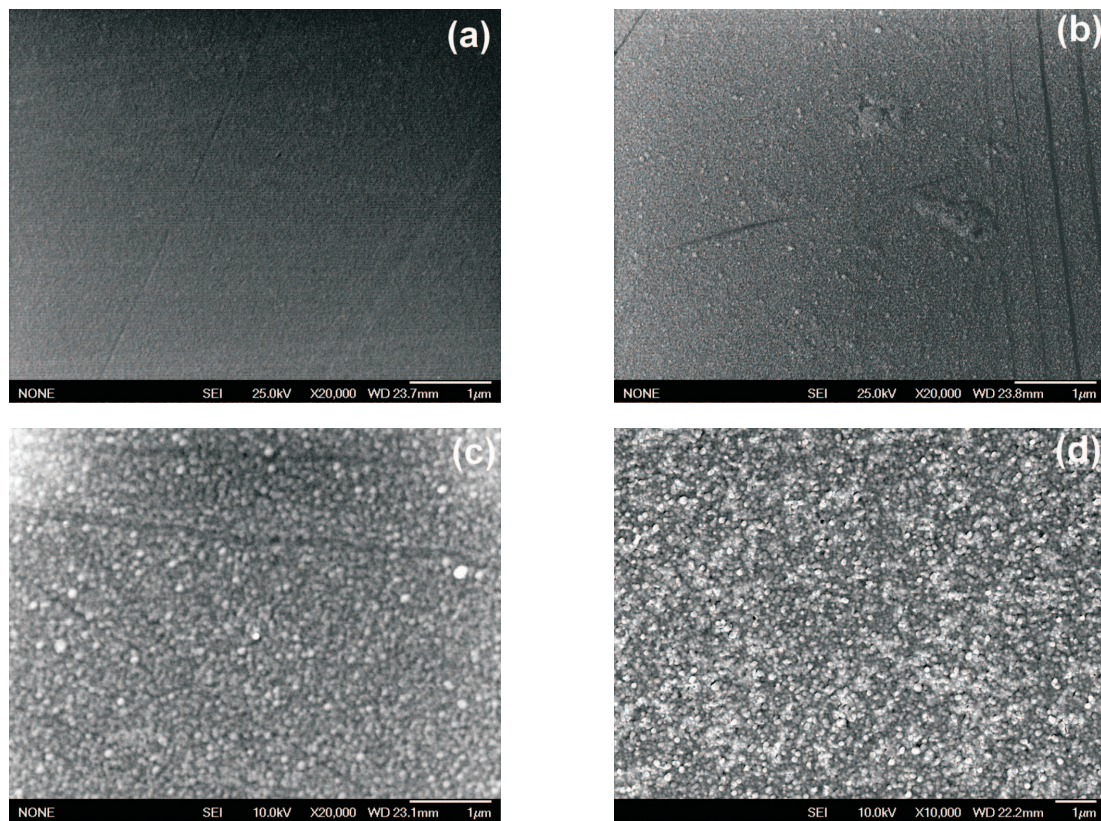


**Fig. 1.** SEM images of the surfaces of films formed by thermo-vacuum coevaporation of the mixtures of silicon and tin powders with tin mass contents of 0 (a), 1 (b), 3 (c), and 5% (d)

of  $\text{Si}_{1-x}\text{Sn}_x$  alloys, as well as the non-uniformity in the distribution of impurities across the film thickness and over the film area, substantially affect the integrated film parameters such as the optical energy gap width, electroconductivity, lifetime and diffusion length of non-equilibrium charge carriers. Ultimately, all those factors become responsible for whether a specific material is suitable for the manufacture of solar cells.

Therefore, this work aimed at studying the microstructure of thin  $\text{Si}_{1-x}\text{Sn}_x$  films fabricated, by using the method of thermo-vacuum coevaporation under the conditions that allow this alloy to be obtained in the form of an amorphous-crystalline composite that includes nano-sized crystals of silicon [14].

## 2. Experimental Technique

Films of  $\text{Si}_{1-x}\text{Sn}_x$  alloy were prepared by thermally coevaporating a mixture of silicon and tin powders in vacuum. The silicon powder was produced by crush-

ing a Si single crystal of the electron purity grade KEF-4.5 and carefully mixed it with a tin powder of grade PO-1 (an Sn content of 99.92%) in various weight ratios. The mixtures were coevaporated from resistive tantalum evaporators in a universal vacuum unit VUP-4 and in a vacuum sputtering installation UVN-2M-1 at a residual gas pressure of about  $2 \times 10^{-5}$  mm Hg. Industrially fabricated polished wafers of single-crystalline silicon and optically pure quartz were used as substrates. Films were deposited at two rates, 5–7 and 15–20 nm/s, onto the substrates with a temperature of 300 °C. The thicknesses of the films obtained, which were determined with the help of an interferometer MII-4, fell within the interval from 250 to 600 nm.

The surface relief of the films was studied with the use of a scanning electron microscope (SEM) JSM-840 at magnifications varying from  $4 \times 10^3$  to  $3 \times 10^4$ .

The chemical composition of near-surface layers in the films was researched, by using an x-ray micro-

probe analyzer CAMEBAX SX50. The profile of impurity distributions across the film thickness was studied in the course of ionic etching with the help of an Auger microprobe Riber Las 2000 with a sensitivity of 0.2 at.%.

The Raman spectra of the films were registered on a spectrometer Jobin Yvon T64000. The spectra were excited by radiation of an Ar-Kr<sup>+</sup> laser with a wavelength of 514.5 nm.

### 3. Results and Their Discussion

The researches of the film surface morphology with the help of SEM showed that the addition of an insignificant amount of tin to the initial silicon powder substantially affects the film surface microstructure. The film surface relief becomes granular (Fig. 1, *b* to *d*). The average grain size grows with the tin content and can reach a value of the order of 100 nm.

The SEM images (Fig. 2) demonstrate that the grains are quasispherical by shape. The researches of their component composition carried out with the help of an x-ray microprobe analyzer showed that the tin content in grains is approximately identical over the whole film surface. At the same time, in grains and grain aggregates that noticeably protrude over the film surface, the contents of oxygen and carbon are 2 to 3 times higher in comparison with those at the plane surface (Fig. 2). In Table 1, the concentrations of main chemical elements at the sites designated in Fig. 2 by figures 1 to 3 are quoted.

From Table 1, one can see that the Sn contents in all tests are approximately identical, whereas the contents of C and O in grain aggregates are 2 to 3 times higher in comparison with the plane surface section. The revealed difference between the distributions of the C and O impurities over the surface can be a result of a larger indraft of those elements, which are present in the composition of residual gases, into nanocrystals, because the latter have a considerably larger surface area in comparison with that of the plane film section. Taking the revealed non-uniformity of impurity distributions at the microscale level into account, the similar measurements of element concentrations over the larger area of the film surface were carried out to make an integrated characterization of the chemical composition of fabricated alloys. The dimensions of the zone scanned by a probe were approximately equal to  $3 \times 3 \mu\text{m}^2$ . The results

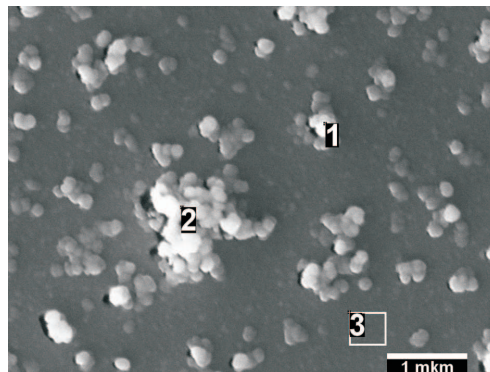


**Fig. 2.** SEM image of the film surface. The numbers mark sites, where the chemical composition of the material was determined: (1) a small aggregate of grains, (2) a large aggregate of grains, and (3) a section free of grains. The square of  $400 \times 400 \text{ nm}^2$  in size shows the microprobe operation region

of measurements are listed in Table 2. When analyzing them, one should pay attention to that the tin content in films is several times higher than that in the initially sputtered mixture Si + Sn. This result can mean that the segregation of tin, which is weakly soluble in silicon, takes place on the film surface in the course of growth of a film.

To determine the distribution of tin atoms across the film thickness, we carried out the Auger analysis

**Table 1. Concentrations of main chemical elements (in at.%) at the sites indicated in Fig. 2**

Number site	Chemical Element			
	C	O	Si	Sn
1	11.88	13.00	74.01	1.11
2	13.92	15.81	69.19	1.08
3	5.22	5.43	87.94	1.41

**Table 2**

Impurity	Specimen's number			
	1	2	3	4
Sn (wt.% of raw material)	0	1.00	3.00	5.00
Sn (wt.% of film)	0	6.56	18.06	22.79
Sn (at.% of film)	0	1.29	3.85	6.12
O (at.% of film)	22.54	46.15	47.64	16.00
C (at.% of film)	0.65	1.54	3.11	0.52

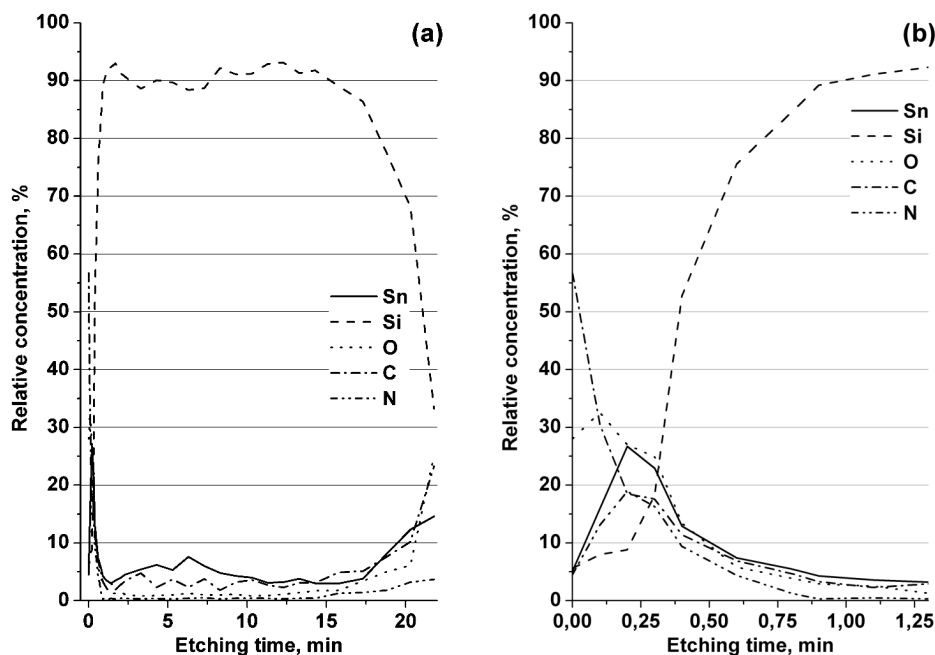


Fig. 3. Dependences of alloy component concentrations across the film thickness (a) and near its surface (b) on the ionic etching duration

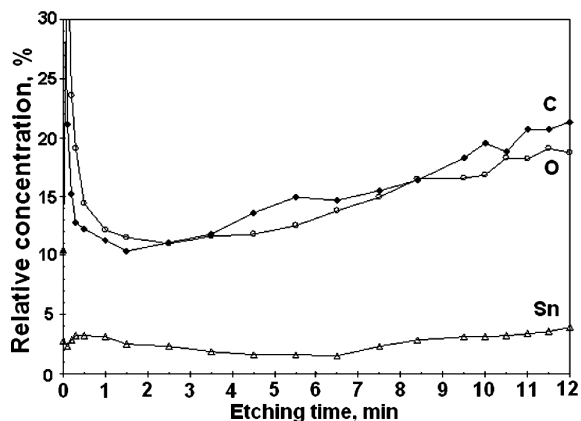


Fig. 4. Dependences of alloy component concentrations across the film thickness on the ionic etching duration

of the film component contents by applying the level-by-level ionic etching. The rate of film sputtering by  $\text{Ar}^+$  ions was 20–25 nm/min. The determination sensitivity of chemical element concentrations was about 0.2 at.%. Some examples of concentration profiles obtained for the distributions of alloy components across the film thickness are depicted in Figs. 3 and 4.

Figure 3 demonstrates the typical profiles of component concentrations across the film formed at a deposition rate of 5–7 nm/s. One can see that the Si–Sn alloy obtained in this way also contains C, N, and O impurities in concentrations that are comparable with that of Sn. In fact, it is a five-component alloy Si–Sn–C–O–N. Moreover, in the external near-surface layer about 5–10 nm in thickness, the concentrations of all impurities in silicon are several times higher than the corresponding concentrations in the film depth. This fact agrees with the results quoted in Table 2 and confirms our assumption concerning the segregation of tin on the film surface during the film growth. A similar character of alloy component concentration distributions across the thickness was observed in the films with a different tin content that were grown up at a rate of 5–7 nm/s. At the same time, when the rate of film formation is 15–20 nm/s, we obtain specimens with a more uniform distribution of the Sn impurity across the film thickness (Fig. 4).

A comparison of the tin distributions across the film thickness that are depicted in Figs. 3 and 4 testifies that the increase of the film growth rate by a factor of three substantially diminishes the oscillations of the Sn concentration, and its near-surface

maximum almost completely disappears from the distribution. However, the increase of the film growth rate gives rise to an increase in the concentrations of technological impurities, carbon and oxygen, over the whole film thickness. This fact evidences that the residual atmosphere in a sputtering chamber is the main source for the indraft of C and O into the alloy for the selected way to fabricate the films. The disappearance of the near-surface maximum from the Sn distribution across the film thickness can be a result of two factors: (i) a reduction of the segregation of this impurity by the film surface owing to increasing the film growth and (ii) the increase of the film surface temperature with of the atomic flux density.

The emergence of a microrelief of such a shape and a scale on the film surface can be associated with the formation of a crystalline silicon phase in the form of clusters of nanocrystals [17]. An efficient method for the diagnostics of a phase state of silicon films is Raman light scattering [18]. In Fig. 5, the Raman spectra of reference films of amorphous silicon deposited in vacuum using the same raw materials, but without the Sn impurity, are shown. The inset of this figure demonstrates the resolution of the Raman spectrum into separate components that have frequencies of 145, 306, 365, and 475  $\text{cm}^{-1}$  and correspond to TA, LA, LO, and TO modes, respectively. The whole spectrum was normalized by the spectrum maximum. From the analysis of the spectra, we arrived at a conclusion that all the films contained only the amorphous phase. Annealing of specimens at temperatures of 450 and 700  $^{\circ}\text{C}$  did not result in the appearance of a crystalline phase, although the frequency positions and halfwidths of the bands changed a little. Such variations testify that the structure of amorphous silicon undergoes the ordering; in other words, the arrangement of silicon atoms approaches the perfect tetrahedral configuration [19]. Notice that even the annealing of a film at 700  $^{\circ}\text{C}$  was not sufficient for the amorphous phase to transform into the crystalline one.

At the same time, films that were doped with tin immediately after their deposition did contain the crystalline phase. Really, from Fig. 6, one can see that the spectra of those films reveal rather a narrow band at about 510  $\text{cm}^{-1}$ , which is typical of nanocrystalline silicon. The analysis of Raman spectra testi-

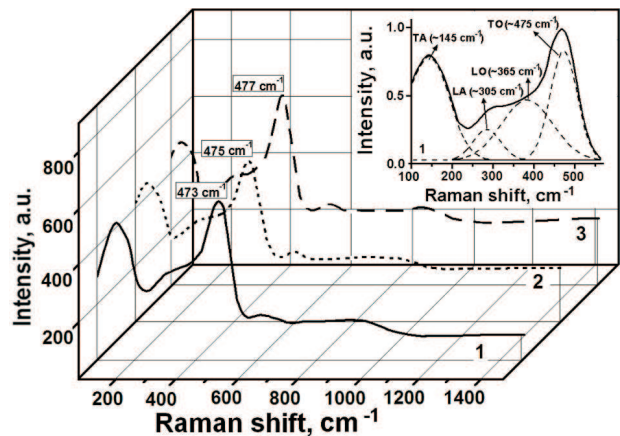


Fig. 5. Raman spectra of reference films not doped with tin: initial (1) and after the 30-min annealing at temperatures of 450 (2) and 700  $^{\circ}\text{C}$  (3)

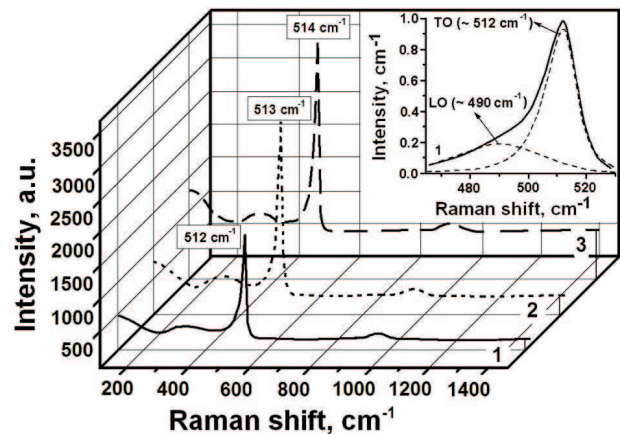


Fig. 6. Raman spectra of Si-Sn alloy films with an Sn content of about 1 at. %: the as-fabricated film (1) and after the 30-min annealing at temperatures of 450 (2) and 700  $^{\circ}\text{C}$  (3)

ties that the annealing of the films concerned gives rise to an increase in the relative fraction of the crystalline phase. The intensity of the band corresponding to nanocrystalline silicon grows, its half-width decreases, and the band itself shifts toward high frequencies.

In order to estimate the fractions of crystalline and amorphous phases in Si:Sn films, we may use the known formula from work [20],

$$X_c = \frac{I_c/I_a}{y + I_c/I_a}, \quad (1)$$

where  $I_c$  and  $I_a$  are the integral intensities of scattering bands of crystalline and amorphous components, respectively; and  $y$  is the ratio between the scattering cross-sections of crystalline and amorphous silicon. The authors of work [20] proposed the following empirical formula to determine the value of  $y$  as a function of the average nanocrystal size  $L$ :

$$y(L) = 0.1 + \exp(-L/25). \quad (2)$$

In turn, the parameter  $L$  can be estimated by the formula [21, 22]

$$I(\nu) = \int \exp\left(-\frac{q^2 L^2}{16\pi^2}\right) \frac{d^3 q}{(\nu - \nu(q))^2 + (\Gamma_0/2)^2}, \quad (3)$$

where  $\Gamma_0$  is the half-width of the phonon band in single-crystalline Si, and  $\nu(q)$  are the dispersion dependences for TO (LO) vibrations.

The resolution of the spectrum in the interval from 400 to 550  $\text{cm}^{-1}$  into a Gaussian component characteristic of amorphous silicon and an asymmetric component described by formula (3) and corresponding to the nanocrystalline phase allowed us to estimate the fraction of each of them. In particular, for the initial film with an Sn content of about 1 at.%, the average dimension of nanocrystals, according to formula (3), amounts to about 3.5 nm. Using this value and formulas (1) and (2), we estimated that the fraction of the crystalline phase in the initial film was equal to 0.85. After the films were annealed at 700 °C for 30 min, this value increased to 0.9.

#### 4. Conclusions

In this work, a combined analysis of the influence of a tin doping on the morphological and structural properties of silicon films fabricated with the use of the method of thermal sputtering of both components is carried out. We have studied the Si films with a concentration of the Sn impurity to be 1–5 wt.% (i.e., 0.2–1.25 at.%). We have found that at least the near-surface layer of a film available for RS-based studies with a wavelength of 514.5 nm is an amorphous crystalline composite. The volume ratio between the crystalline and amorphous phases in the films depends on the integral concentration of the tin impurity and the specimen annealing temperature. In particular, in unannealed films with the integral content of Sn near 1 at.%, the fraction of the crystalline phase amounts to 85%. The prevailing size of silicon nanocrystals in

the amorphous matrix of a film is 3.5 nm. The microstructure of film surfaces was characterized by the granular relief with grains of a quasispherical shape. The grain dimensions substantially depend on the tin content and can reach 100 nm. The researches of component contents at the film surfaces reveal a uniform distribution of tin over them. No metal clusters or other precipitations with an elevated content of tin are revealed. The distributions of Sn and technological impurities (C, O, and N) across the film thickness are uniform except those in a near-surface layer 10–20 nm in thickness. The degree of impurity distribution uniformity across the film thickness is determined to depend on the rate of film growth. This should be taken into account at the interpretation of the results of RS-based studies. The films fabricated under the same conditions, but without tin doping, had similar distributions of technological impurities, but were completely amorphous, and the granularity of their surface relief was not observed.

Our results testify to the ability of the tin impurity to efficiently stimulate the formation of silicon nanocrystals in the amorphous matrix of silicon films during their formation. The nanocomposite obtained by the described method can be of interest for the application in photo-electric energy converters.

*The work was partially supported in the framework of the State goal-oriented scientific and technical program “Nanotechnologies and nanomaterials” and the Ukrainian-Russian program for the development of cooperation in nanotechnologies.*

*The authors are grateful to V. Voitovych, A. Kolosyuk, and R. Rudenko for fabricating the specimens and plotting the results obtained.*

1. Zh.I. Alferov, V.M. Andreev, and V.D. Rumyantsev, *Semiconductors* **38**, 899 (2004).
2. N.S. Lewis, *Science* **315**, 798 (2007).
3. M.A. Green, K. Emery, Y. Hishikawa, and W. Warta, *Prog. Photovolt. Res. Appl.* **19**, 84 (2011).
4. J. Ahn, K. Jun, and K. Lim, *Appl. Phys. Lett.* **82**, 1718 (2003).
5. A.V. Shah, H. Schade, M. Vanesek et al., *Prog. Photovolt. Res. Appl.* **12**, 113 (2004).
6. D. Girginoudi, N. Georgoulas, and F.J. Thanailakis, *J. Appl. Phys.* **66**, 354 (1989).
7. A. Mohamedi, M.L. Thève, M. Vergnat, G. Marchal, and M. Piecuch, *Phys. Rev. B* **39**, 3711 (1989).
8. G.N. Parsons, J.W. Cook, G. Lucovsky, S.Y. Lin, and M.J. Mantini, *J. Vac. Sci. Technol. A* **4**, 470 (1986).

9. D.L. Williamson, C.R. Kerns, and S.K. Deb, *J. Appl. Phys.* **55**, 2816 (1984).
10. R. Ragan, K.S. Min, and H.A. Atwater, *Mater. Sci. Eng. B* **87**, 204 (2001).
11. A.J. Kurt and N.W. Ashcroft, *Phys. Rev. B* **54**, 14480 (1996).
12. M. Vergnat, M. Piecuch, G. Marchal, and M. Gerl, *Philos. Mag. B* **51**, 327 (1985).
13. S.Yu. Shiryaev, J.L. Hansen, P. Kringhøj, and A.N. Larsen, *Appl. Phys. Lett.* **67**, 2287 (1995).
14. V.V. Voitovych, V.B. Neimash, N.N. Krasko, A.G. Koliusiuk, V.Yu. Povarchuk, R.M. Rudenko, V.A. Makara, R.V. Petrunya, V.O. Juhimchuk, and V.V. Strelchuk, *Semiconductors* **45**, 1281 (2011).
15. C. Claeys, E. Simoen, V.B. Neimash, A. Kraitchinskii, M. Krasko, O. Puzenko, A. Blondeel, and P. Clauws, *J. Electrochem. Soc.* **148**, G738 (2001).
16. V.B. Neimash, V.V. Voitovych, A.M. Kraichynskiy, L.I. Shpinar, M.M. Krasko, V.M. Popov, A.P. Pokanevych, M.I. Gorodynskiy, Yu.V. Pavlovskiy, V.M. Tsmots, and O.M. Kabaldin, *Ukr. Fiz. Zh.* **50**, 492 (2005).
17. J. Koh, A.S. Ferlauto, P.I. Rovira, R.J. Koval, C.R. Wronski, and R.W. Collins, *J. Non-Cryst. Solids* **266-269**, 43 (2005).
18. E.I. Terukov, V.Kh. Kudoyarova, V.Yu. Davydov *et al.*, *Mater. Sci. Eng. B* **69-70**, 266 (2000).
19. R. Tsu, *J. Non-Cryst. Solids* **97-98**, 163 (1988).
20. E. Bustarret, M.A. Hachicha, and V. Brunel, *Appl. Phys. Lett.* **52**, 1675 (1978).
21. H. Richter, Z.P. Wang, and L. Ley, *Solid State Commun.* **39**, 625 (1981).
22. H. Cambell and P.M. Fauchet, *Solid State Commun.* **58**, 739 (1986).

Received 15.11.12.

Translated from Ukrainian by O.I. Voitenko

*В.Б. Неймаш, В.М. Порошин, О.М. Кабалдин,  
В.О. Юхимчук, П.Є. Шепелявий,  
В.А. Макара, С.Ю. Ларкін*

#### МІКРОСТРУКТУРА ТОНКИХ КОМПОЗИТНИХ ПЛІВОК Si-Sn

#### Резюме

Методами оже та раманівської спектроскопії, рентгенівського флуоресцентного аналізу та електронної мікроскопії досліджено особливості мікроструктури тонких плівок сплаву Si-Sn, виготовлених термовакуумним співвипаровуванням Si та Sn. Досліджено властивості плівок з вмістом Sn в інтервалі від 1 до 5 вагових відсотків. Встановлено суттєвий вплив олова на формування мікрорельєфу поверхні плівок та нанокристалів у аморфній матриці. Квазісферичні утворення на поверхні плівок можуть сягати розмірів порядку 100 нм. Частка нанокристалічної кремнієвої фази в плівці може досягати 90% її об'єму. Проаналізовано роль умов та швидкості росту плівок у розподілі концентрації Sn та технологічних домішок C і O по поверхні та товщині плівок.